CETLIN, B. B. & ABRAHAMS, S. C. (1963). *Acta Cryst.* **16**, 943.
CROMER, D. T. (1965). *Acta Cryst.* **18**, 17.
CROMER, D. T. & WABER, J. T. (1965). *Acta Cryst.* **18**, 104.
FRITCHIE, C. J. (1967). Unpublished. Program later modified by L. GUGGENBERGER and by P. B. JAMIESON.
HAMILTON, W. C. & ABRAHAMS, S. C. (1970). *Acta Cryst.* A**26**, 18.
KRIZ, H. M. & BRAY, P. J. (1969). *J. Chem. Phys.* **51**, 3624.
LEVIN, E. M., ROTH, R. S. & MARTIN, J. B. (1961). *Amer. Min.* **46**, 1030.
MAREZIO, M., REMEIKA, J. P. & DERNIER, P. D. (1969). *Acta Cryst.* B**25**, 955.
SHANNON, R. D. & PREWITT, C. T. (1969). *Acta Cryst.* B**25**, 925.
SHANNON, R. D. & PREWITT, C. T. (1970). *Acta Cryst.* B**26**, 1046.
ZACHARIASEN, W. H. (1963). *Acta Cryst.* **16**, 1139.

J. Appl. Cryst. (1971). **4**, 290

Small-Angle X-ray Scattering from Helical Macromolecules*

BY O. ALLAN PRINGLE AND PAUL W. SCHMIDT

Physics Department, University of Missouri, Columbia, Missouri 65201, *U.S.A.*

(*Received* 10 *December* 1970; *accepted* 11 *February* 1971)

An earlier calculation of the intensity of small-angle X-ray scattering from helical filaments is extended to give an expression for the intensity from helical macromolecules with a finite cross section. The results are in quite good agreement with an experimental scattering curve for a solution of DNA molecules.

Introduction

Small-angle X-ray scattering is often useful for studying the overall form and dimensions of biological macromolecules. Although this information about the macromolecule can also be obtained from a complete determination of the crystal structure, small-angle X-ray scattering can be applied to macromolecules which cannot be crystallized or for which a complete structure analysis has not been carried out. Also, information about the overall configuration of the macromolecule can be obtained more easily by small-angle scattering than by a crystal structure determination. Moreover, small-angle X-ray scattering permits molecules to be studied when they are actually in suspension. Suspended molecules at times can have a configuration which is different from the molecular shape in the crystal.

Helical configurations are important in the study of biological macromolecules. One of us has recently calculated the small-angle X-ray scattering from dilute suspensions of randomly oriented helical filaments (Schmidt, 1970). To simplify the calculation, only filaments were considered. However, a more realistic calculation would take account of the finite cross section of the helixes.

Below, we describe a method by which the previous calculation can be extended to give the scattered intensity from macromolecules made up of two identical coaxial helixes with finite cross sections.

* Work supported by the National Science Foundation and by the Department of Defense Project Themis.

Calculation of the scattered intensity

Except for having a finite cross section, the molecules will be assumed to satisfy the same assumptions as in the earlier calculation. The electron density of the molecules will be considered to be uniform, and the particles will be assumed to be identical, independent, and randomly oriented. The measured scattering will be taken to be the scattered intensity averaged over all particle orientations. Under these assumptions, the scattering from the system of particles will be proportional to the scattering from a single particle. Since we will be concerned only with the angular dependence of the scattered intensity, we will calculate only the scattering from a single particle.

With the above assumptions, the scattered intensity is the average, over all particle orientations, of the square of the structure factor for a helical macromolecule.

For a single helical filament with a given orientation, the structure factor $F_f(h, \alpha, \Psi)$ is given by (Schmidt, 1970, equation (7) with $\varphi=0$) as

$$F_f(h,\alpha,\Psi)=\sum_{n=-\infty}^{\infty}\exp\{in(\pi/2-\Psi)F_n(h,\alpha)\exp\{i(H/2)(h\cos\alpha+2\pi n/P)\} \quad (1)$$

where

$$h=4\pi\lambda^{-1}\sin(\theta/2)$$

$$F_n(h,\alpha)=J_n(hR\sin\alpha)\frac{\sin[(H/2)(h\cos\alpha+2\pi n/P)]}{(H/2)(h\cos\alpha+2\pi n/P)}$$

and where λ is the X-ray wavelength, θ is the scattering angle, α is the angle between the helix axis and the vector

$\mathbf{s}-\mathbf{s}_0$, $\mathbf{s}$ and $\mathbf{s}_0$ are unit vectors in the directions of the scattered and incident rays, Ψ is an azimuth angle which gives the orientation of the helix about a reference axis parallel to the helix axis, $J_n(x)$ is the Bessel function of the first kind and order n, H is the length of the helix, P is the helix period, and R is its radius. The helix thus consists of H/P turns. The ratio H/P, which need not be an integer, will be assumed to be large, and the calculation will be carried out only for a helix which can be considered infinitely long.

A helix with a finite cross section will be constructed from an assembly of coaxial helical filaments with the same length but with different azimuth angles Ψ and radii r. The structure factor $F(h,\alpha,\psi)$ for a particle consisting of two identical coaxial helixes with a finite cross section then can be written

$$F(h,\alpha,\Psi)=\frac{\int_{aR}^{R} r\,dr \int_{\theta_1(r)}^{\theta_2(r)} D(r,\theta)[F_f(h,\alpha,\theta+\Psi)+F_f(h,\alpha,\theta+\varphi+\Psi)]\,d\theta}{2\int_{aR}^{R} r\,dr\int_{\theta_1(r)}^{\theta_2(r)} D(r,\theta)\,d\theta} \tag{2}$$

where r and θ are polar coordinates in a plane perpendicular to the helix axis; r, aR, $\theta_2(r)$, and $\theta_1(r)$ define the form of the helix cross section in a plane perpendicular to the helix axis; φ is the angle by which one helix is rotated with respect to the other; and $D(r,\theta)$ describes the density of filaments in the plane of the helix cross section.

For simplicity, θ_1, θ_2, and the density $D(r,\theta)$ will be assumed to be constant, with $\theta_1=0$ and $\theta_2=\omega$. The particle cross section is shown in Fig. 1. For this cross section, by substitution of (1) in (2), $F(h,\alpha,\Psi)$ can be written

$$F(h,\alpha,\Psi)=\sum_{n=-\infty}^{\infty} E_n(h,\alpha,\Psi)\frac{\sin(n\omega/2)}{(n\omega/2)} \times\cos(n\varphi/2)G_n(h,\alpha) \tag{3}$$

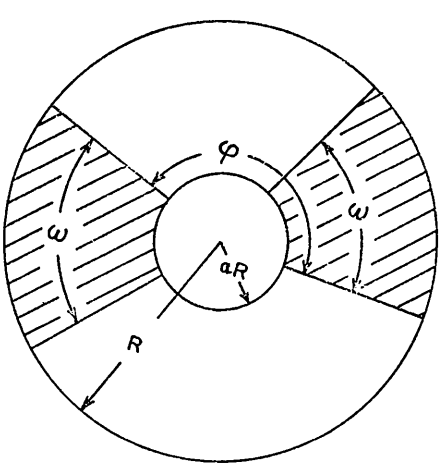

Fig. 1. A diagram of the particle cross section. Cross-hatching indicates the area occupied by the two helixes.

where

$$E_n(h,\alpha,\Psi)=\exp\{i\pi/2-\omega/2-\varphi/2-\Psi) \times\exp\{i(H/2)(h\cos\alpha+2\pi n/P)\}$$

$$G_n(h,\alpha)=\frac{\int_{aR}^{R} rF_n(h,\alpha)\,dr}{\frac{1}{2}R^2(1-a^2)}.$$

The scattered intensity $I(h)$ is the intensity averaged over all particle orientations. Therefore

$$I(h)=\frac{1}{4\pi}\int_0^{2\pi} d\Psi\int_0^{\pi} d\alpha\sin\alpha F(h,\alpha,\Psi)F^*(h,\alpha,\Psi). \tag{4}$$

In (4), the values of $F(h,\alpha,\Psi)$ and its complex conjugate $F^*(h,\alpha,\Psi)$ are obtained from (3). The intensity is normalized so that $I(0)=1$.

The integrand in (4) is a double sum. However, in the integration over Ψ, all terms in this double sum average to zero unless the terms are independent of Ψ. The double sum therefore reduces to a single sum. If $\varepsilon_0=1$ and $\varepsilon_n=2$ for $n\geq 1$, (4) can be written

$$I(h)=\sum_{n=0}^{\infty}\varepsilon_n\cos^2(n\varphi/2)\frac{\sin^2(n\omega/2)}{(n\omega/2)^2} \times\tfrac{1}{2}\int_0^{\pi}\sin\alpha\,d\alpha\,[G_n(h,\alpha)]^2.$$

For a long helix, $F_n(h,\alpha)$, and consequently $G_n(h,\alpha)$, will be appreciably different from zero only when $h\cos\alpha+2\pi n/P=0$. Thus, for an infinitely long helix,

$$I(h)=\frac{\pi}{hH}\sum_{n=0}^{\infty}\varepsilon_n\cos^2(n\varphi/2)\frac{\sin^2(n\omega/2)}{(n\omega/2)^2}[g_n(hR,a)]^2 \tag{5}$$

where

$$g_n(hR,a)=2R^{-2}(1-a^2)^{-1}\int_{aR}^{R} dr\,r\,J_n(hr\sqrt{1-q_n^2})$$

and where

$$b=2\pi R/P$$
$$q_n=nb/hR \quad hR\geq nb$$
$$q_n=1 \quad hR\leq nb$$

Although (5) is written as an infinite series, the number of terms actually is finite, since all terms are zero for $n\geq hR/b$.

Numerical calculations

For evaluation of (5), the $g_n(hR,a)$ were expanded in the power series

$$g_n(hR,a)=\sum_{k=0}^{\infty}c_{kn}(hR)\,S_{kn}(a) \tag{6}$$

where

$$c_{kn}(hR) = \frac{(-1)^k (hR\sqrt{1-q_n^2})^{n+2k}}{k!\,(n+k)!\,2^{n+2k}},$$

$$S_{kn}(a) = \frac{2[1-a^{n+2k+2}]}{(1-a^2)(n+2k+2)}.$$

A Fortran IV program was written for calculating $I(h)$ from (5) and (6) on an IBM 360–60 computer. Intensity values were obtained for $0{\cdot}1 \le hR \le 15{\cdot}0$ with an increment of 0·1 for different values of the parameters a, b, ω, and φ. Copies of the program are available from the authors.

Discussion

The calculated intensities were compared with an experimental scattering curve for a suspension of DNA molecules (Bram & Beeman, 1971). The parameters of the DNA molecule (Mahler & Cordes, 1966) suggest that φ is about 2·2 radians and that b is roughly equal to 2. In almost all of the calculations, therefore, φ and b were near 2·2 radians and 2, respectively.

Comparison of the experimental and calculated curves definitely indicated that fits could be obtained only when $0{\cdot}8 \le \omega \le 1{\cdot}5$.

For a given choice of a, b, φ and ω, the outer radius R was found by multiplying $I(hR)$ and hR by the constants which gave the best fit of the calculated and theoretical experimental curves.

The parameter a was found to determine the ratio of the intensity of the first subsidiary maximum to the zero-angle intensity. (For filaments, $a=1{\cdot}0$) In the earlier calculation of the intensity from helical filaments with dimensions corresponding to those of the DNA molecule (Schmidt, 1970, Fig. 8), the intensity of the first subsidiary maximum of the calculated curve is higher than the measured intensity when the inner parts of the curves are made to coincide. Trials with several values of a soon showed clearly that a must be less than 0·1 to fit the data. Therefore, in the last part of the calculation, a was set equal to zero.

Our calculations thus indicate that the theoretical curve which fits the data must correspond to a helical molecule with a solid center. This result agrees with current models of the DNA B structure. (Mahler & Cordes, 1966).

While the number of parameters is so large that an evaluation of the sensitivity of the results to changes in the parameters is somewhat subjective, our tests suggest that $0 \le a \le 0{\cdot}1$, $0{\cdot}8 \le \omega \le 1{\cdot}2$, $1{\cdot}8 \le b \le 2{\cdot}2$, and $2{\cdot}0 \le \varphi \le 2{\cdot}4$.

Fig. 2 shows the calculated curve which best fits the data. For the computed curve, $R=11{\cdot}5$ Å, $a=0$, $\varphi=2{\cdot}26$ radians, $\omega=1{\cdot}00$ radians, and $b=2{\cdot}13$.

The agreement between the experimental and calculated curves can be considered quite satisfying, especially when consideration is taken of the fact that our model of a uniform-density helix is a great simplification of the actual DNA structure. Agreement between the calculated and measured curves should not be expected in the angular region beyond the first two subsidiary maxima, since the detailed molecular structure undoubtedly affects this part of the curve.

In Fig. 2, the experimental and calculated curves differ somewhat in the neighborhood of 2×10^{-2} radians. In this angular region the scattering is changing from the h^{-1} dependence which is observed in the inner part of the scattering curve and which is expected for an infinitely long rod in this portion of the curve. For scattering angles greater than about 2×10^{-2} radians, the dimensions of the cross section no longer can be considered negligible and the intensity near 2×10^{-2} radians is determined primarily by the form of the cross section. The difference between the calculated and experimental curves in this region of angles probably results from the fact that the assumed dimensions and electron density of the cross section do not correspond sufficiently closely to the actual values in DNA. Further calculations would be required before more detailed statements could be made about the reasons for these deviations.

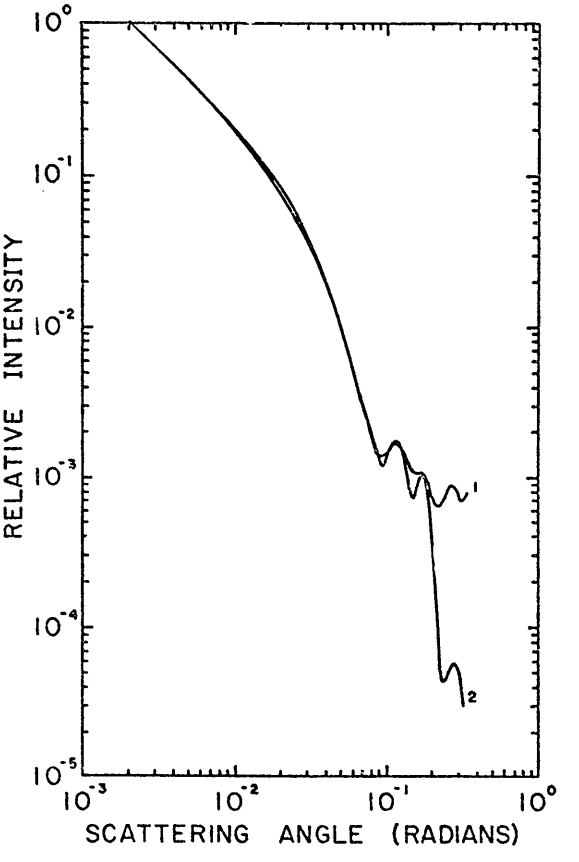

Fig. 2. Curve 1 represents the scattered intensity for a DNA solution (Bram & Beeman, 1971). Curve 2 is calculated from equation (5) for $R=11{\cdot}5$ Å, $a=0$, $\varphi=2{\cdot}26$ radians, $\omega=1{\cdot}00$ radians, $b=2{\cdot}13$.

With relatively little difficulty, our equations could be generalized to permit intensity calculations for other cross-sectional shapes and for cross sections with non-uniform electron density.

When $\varphi=\omega=\pi$ and $a=0$, the helix becomes a cylinder with uniform electron density. Then in (5) only the term for $n=0$ is different from zero, and (5) reduces to the expression for the intensity from a very long uniform cylinder [Fedorov & Aleshin, 1966, equation (10)].

We thank W. W. Beeman for his helpful suggestions and advice.

References

BRAM, S. & BEEMAN, W. W. (1971). *J. Mol. Biol.* **55**, 317.
FEDOROV, B. A. & ALESHIN, V. G. (1966). *Vysokomol. Soed.* **8**, 1508. English Translation: *Polymer Phys. USSR*, (1967). **8**, 1660.
MAHLER, H. R. & CORDES, E. H. (1966). *Biological Chemistry*, p. 141. New York: Harper & Row.
SCHMIDT, P. W. (1970). *J. Appl. Cryst.* **3**, 257.

J. Appl. Cryst. (1971). **4**, 293

A High-Temperature X-ray Diffraction Study of the NiO – Li_2O System

BY C. J. TOUSSAINT

Chemistry Division, Euratom C.C.R., Ispra, Italy

(*Received* 1 *February* 1971; *accepted* 22 *March* 1971)

A crystallographic study of the system $Ni^{2+}_{1-2x}Ni^{3+}_{x}Li^{+}_{x}O$ has been carried out. The crystal structure of the material in the range $0\leq x\leq 0{\cdot}4$ at room temperature and up to 1000 °C has been studied. The principal coefficients of thermal expansion and the phase diagram are given. The structural rhombohedral → face-centred cubic transition temperature of NiO has been determined.

Introduction

Verwey, Haaijman, Romeijn & van Oosterhout (1950) have shown that when lithium oxide is substitutionally inserted into nickel oxide, a solid solution has been formed. The substitution is accompanied by the oxidation of an equivalent amount of the transition metal to the trivalent state. Thus the formula may be written as $Ni^{2+}_{1-2x}Ni^{3+}_{x}Li^{+}_{x}.O$ Concerning the system of oxides, only structural studies at room temperature seem to have been reported (Brownlee & Mitchell, 1952; Goodenough, Wickham & Croft, 1958; Bade, Bronger & Klemm, 1965; Bronger, Bade & Klemm, 1964; Gallezot, Degraix & Gravelle, 1969).

This communication deals with an X-ray room- and high-temperature study, up to 1000 °C, of materials with compositions $0\leq x\leq 0{\cdot}4$.

Experimental

Lithium-doped nickel oxide was prepared by sintering mixtures of nickel oxide and lithium peroxide (Li_2O_2) at 1000 °C in closed Pt crucibles to prevent excessive losses of lithium and of oxygen. The nickel oxide was prepared by thermal decomposition of doubly crystallized nickel sulphate (Merck p.a.) and by annealing the decomposition product at 1100 °C in oxygen (Geel, Morlotti & Pizzini, 1970). The lithium content of the NiO obtained in this way was less than 30 ppm. The nickel-to-oxygen ratio was 1·005. For the determination of the crystallographic transition temperature and thermal expansion of pure NiO, a sample obtained from Schlesinger (purity 99·99 %, NiO ratio 0·999) has also been used. Lithium has been determined byflame emission spectroscopy and by X-ray diffraction measurements (Toussaint & Vos, 1968). Compositions $Ni^{2+}_{1-2x}Ni^{3+}_{x}Li^{+}_{x}O$ with $0\leq x\leq 0{\cdot}4$ have been prepared by this method.

The room-temperature (22 °C) X-ray measurements were carried out on a Philips diffractometer, using nickel-filtered Cu $K\alpha$ ($\lambda=1{\cdot}5418$ Å) radiation. Lattice parameters were calculated by means of the $2\bar{1}1$, 321, $2\bar{1}\bar{1}$–310 and 332 reflexions for the rhombohedral structure, and the 420 and 422 reflexions for the cubic structure, with platinum as internal standard. All reflexions were well resolved into α_1 and α_2. The reflexions were recorded using a xenon-filled proportional counter. The usual scanning speed was $\frac{1}{8}°\ 2\theta.\text{min}^{-1}$.

The X-ray patterns for the lattice expansion measurements and crystallographic transformation temperatures were carried out on a Rigaku high-temperature X-ray diffractometer attachment (air atmosphere) in combination with an automatic temperature controller. Sample temperatures were determinated with a Pt–$Pt_{87}Rh_{13}$ thermocouple, calibrated with platinum, using the data of Lang & Franklin (1964). Subsequent temperature calibrations have shown that the temperatures are correct to ±4 °C near 200 °C, and to ±8 °C near 1000 °C. To exclude errors in the temperature measurements owing to a difference in thermal conductivity between NiO and Pt (calibration standard), the crystallographic transition temperature of NiO has